New Journal of Physics
The open access journal at the forefront of physics

Deutsche Physikalische Gesellschaft DPG
IOP Institute of Physics

Published in partnership with: Deutsche Physikalische Gesellschaft and the Institute of Physics

CrossMark

OPEN ACCESS

RECEIVED
11 January 2016

REVISED
4 April 2016

ACCEPTED FOR PUBLICATION
19 April 2016

PUBLISHED
6 May 2016

Original content from this work may be used under the terms of the Creative Commons Attribution 3.0 licence.

Any further distribution of this work must maintain attribution to the author(s) and the title of the work, journal citation and DOI.

PAPER

Nonlinear plasmonics in a two-dimensional plasma layer

Bengt Eliasson[1,3] **and Chuan Sheng Liu**[2]

[1] SUPA, Physics Department, John Anderson Building, University of Strathclyde, Glasgow G4 0NG, Scotland, UK
[2] Chou Kuang Piu College, University of Macau, Avenida da Universidade, Taipa, Macau, People's Republic of China
[3] Author to whom any correspondence should be addressed.

E-mail: bengt.eliasson@strath.ac.uk **and** csliu@umac.mo

Keywords: two-dimensional plasmons, modulational instability, rogue waves, graphene, sheet of electrons

Abstract

The nonlinear electron dynamics in a two-dimensional (2D) plasma layer are investigated theoretically and numerically. In contrast to the Langmuir oscillations in a three-dimensional (3D) plasma, a well-known feature of the 2D system is the square root dependence of the frequency on the wavenumber, which leads to unique dispersive properties of 2D plasmons. It is found that for large amplitude plasmonic waves there is a nonlinear frequency upshift similar to that of periodic gravity waves (Stokes waves). The periodic wave train is subject to a modulational instability, leading to sidebands growing exponentially in time. Numerical simulations show the breakup of a 2D wave train into localized wave packets and later into wave turbulence with immersed large amplitude solitary spikes. The results are applied to systems involving massless Dirac fermions in graphene as well as to sheets of electrons on liquid helium.

1. Introduction

Two-dimensional (2D) conducting layers have unique plasmonic properties, where the wave frequency of low-energy plasmons (in the long wavelength limit) typically depends on the square root of the wavenumber, and observed 2D plasmons have wave-frequencies most commonly in the THz range or below. Examples of experimental observations include 2D plasmons in a sheet of electrons on liquid helium [1], in silicon inversion layers [2], monolayer graphite [3], single layer graphene on SiC substrates [4, 5], epitaxial graphene [6], etc. Graphene has unique electronic and material [7–10] properties, and plasmons in graphene is now a field of intense research with important applications in optics, electronics, metamaterials, light harvesting, energy storage, THz technology, and so on [11, 12]. Experiments have shown that Dirac plasmons in graphene on SiC are hybridized with optical phonons of the SiC substrate [13], while scattering of plasmons off capillary waves (riplons) were observed in an electron sheet on liquid helium [1]. Nonlinear photonics have important applications in graphene with respect to harmonic generation [14], optical and plasmonic bistability [15, 16], broadband optical limiting application [17], four-wave mixing frequency conversion [18], and other nonlinear photonic applications [19]. On the other hand, the self-interaction among large amplitude 2D plasmons and their sidebands could be an important source of instability and localization of wave energy. For example, the instability of large amplitude plasma waves have been suggested to lead to 'rogue waves' in semiconductor plasmas [20], and optical rogue waves have been observed in semiconductor lasers [21] and other optical systems [22, 23]. It has also been proposed that graphene supports optical solitons in a graphene monolayer [24], dissipative plasmon solitons in multilayer graphene [25] and graphene nanodisk arrays [26].

The aim of this paper is to theoretically and numerically investigate the nonlinear behavior of large-amplitude plasmons in a 2D plasma layer. The basic fluid equations are presented and motivated in section 2. As discussed in section 3, the unique dispersive properties of 2D plasmons lead to a similar behavior to surface gravity waves [27–29], such as a nonlinear upshift of the frequency due to harmonic generation, and a modulational instability resulting in the growth of sidebands of the periodic wavetrain. In section 4, the theoretical results are compared with a direct numerical simulation of the dynamic system, which also

© 2016 IOP Publishing Ltd and Deutsche Physikalische Gesellschaft

demonstrates the breakup of the periodic wavetrain into localized envelope solitary waves and later into spiky large amplitude structures immersed in wave turbulence. Numerical examples are given for systems involving massless Dirac fermions in graphene and for sheets of electrons on liquid helium. Finally, some conclusions are drawn in section 4.

2. Nonlinear fluid model of a two-dimensional plasma layer

Low-energy plasmons, i.e. in the long wavelength and low-frequency limit, may be studied using a hydrodynamic model [11, 30], in which the conservation of electrons (charges) is governed by a continuity equation and their fluid velocity (or alternatively the current density) by a momentum equation. Due to the dynamics of the electrons in a 2D sheet of plasma, the electrostatic potential, which extends also to the out-of-plane dimension, has a particular form which leads to a unique dispersive behavior of the system. The potential is obtained from Poisson's equation with the electron density concentrated to a 2D plane, and is given by

$$\phi(\mathbf{r}, t) = -\frac{e}{4\pi\epsilon_0\epsilon}\int\frac{(n_e(\mathbf{r}', t) - n_0)}{|\mathbf{r} - \mathbf{r}'|}\mathrm{d}^2r', \tag{1}$$

where the integral is taken over the 2D plane of the plasma layer. Here n_e is the areal electron number density, n_0 represents the neutralizing ion background density, e is the magnitude of the electron charge, ϵ_0 is the electric vacuum permittivity, and ϵ is the mean dielectric constant of the surrounding medium [11]. We choose a coordinate system such that the plasma layer is in the x-y plane. For a plane wave, where the electron density given by $n_e = n_0 + n_{e1}$ with $n_{e1} = (1/2)\hat{n}_e\exp(-\mathrm{i}\omega t + \mathrm{i}\mathbf{k}\cdot\mathbf{r}) +$ complex conjugate, and the potential $\phi = (1/2)\hat{\phi}\exp(-\mathrm{i}\omega t + \mathrm{i}\mathbf{k}\cdot\mathbf{r}) +$ complex conjugate, the Fourier component of the potential is obtained from equation (1) as

$$\hat{\phi} = -\frac{1}{2k}\frac{e}{\epsilon_0\epsilon}\hat{n}_e, \tag{2}$$

where $k = \sqrt{k_x^2 + k_y^2}$ is the magnitude of the wave vector. The factor $1/(2k)$ in equation (2) leads to significantly different behavior of 2D plasmons compared to the three-dimensional (3D) case, where the corresponding factor $1/k^2$ gives rise to Langmuir oscillations. The electron dynamics is governed by the continuity and momentum equation

$$\frac{\partial n_e}{\partial t} + \nabla_\perp\cdot(n_e\mathbf{v}_e) = 0, \tag{3}$$

and

$$\frac{\partial \mathbf{v}_e}{\partial t} + (\mathbf{v}_e\cdot\nabla_\perp)\mathbf{v}_e = \frac{4\epsilon_0 D}{en_0}\nabla_\perp\phi, \tag{4}$$

respectively, where $\mathbf{v}_e = \hat{\mathbf{x}}v_{ex} + \hat{\mathbf{y}}v_{ey}$ is the electron fluid velocity, $\hat{\mathbf{x}}$ and $\hat{\mathbf{y}}$ are unit vectors in the x and y-directions, D is the Drude weight [11, 31], n_0 is the mean electron density, and the gradient operator $\nabla_\perp = \hat{\mathbf{x}}\partial/\partial x + \hat{\mathbf{y}}\partial/\partial y$. Equations (3) and (4) are coupled through the potential ϕ in equation (1). For Schrödinger electrons with effective mass m_b, the Drude weight (in SI units) is $D = e^2n_0/(4\epsilon_0 m_b)$, while for massless Dirac fermions, the Drude weight is $D = e^2E_F/(4\pi\epsilon_0\hbar^2)$, where the Fermi energy is $E_F = \hbar v_F k_F$, $v_F \approx 10^6\mathrm{ms}^{-1}$ is the Fermi speed, and $k_F = \sqrt{\pi n_0}$ is the Fermi wavenumber.

For analytic convenience in the following section, we assume irrotational potential flow, $\mathbf{v}_e = \nabla_\perp\psi_e$, where ψ_e is the flow potential, which inserted into equations (3) and (4) gives the two scalar equations,

$$\frac{\partial n_e}{\partial t} + \nabla_\perp\cdot(n_e\nabla_\perp\psi_e) = 0, \tag{5}$$

and

$$\frac{\partial \psi_e}{\partial t} + \frac{1}{2}(\nabla_\perp\psi_e)^2 = \frac{4\epsilon_0 D}{en_0}\phi + B(t), \tag{6}$$

for the unknowns n_e and ψ_e. Equations (1), (5) and (6) are coupled systems for ϕ, n_e and ψ_e. In equation (6), $B(t)$ is an arbitrary function of time, which we can choose to set to zero, since the fluid velocity $\mathbf{v}_e$ is the spatial gradient of ψ and will not depend on $B(t)$, and hence, $B(t)$ will not influence the dynamics of n_e. The nonlinearity $(\nabla_\perp\psi_e)^2/2$ in equation (6) can also give rise to a mean component of ψ_e depending only on time, which likewise will not contribute to the dynamics of the system.

3. Nonlinear wave-wave interactions

Two major nonlinear effects of large amplitude plasmons are here investigated theoretically: a nonlinear frequency upshift due to harmonic generation, and a modulational instability of the wavetrain leading to sidebands growing exponentially in time during the linear phase. These effects have been investigated in the past with respect to general nonlinear dispersive media [32, 33], plasma waves [34–39], and nonlinear water waves [28]. A full investigation of the nonlinear system would involve the following steps: i) to find the profile of the nonlinear periodic wavetrain governed by equations (5)–(6) and the corresponding nonlinear frequency (or phase velocity) depending on the wavelength and amplitude. This wavetrain would form a 'lattice' on which small-amplitude, unstable sidebands in the form of Bloch waves $F(\theta_0)\exp(i\theta_s)$, can develop, where θ_0 and θ_s are carrier and perturbation phases (see definitions below), and $F(\theta_0)$ is periodic with respect to its argument. ii) To derive a linearized system of differential equations for the Bloch functions $F(\theta_0)$ and corresponding perturbation frequencies Ω. The set of Bloch functions for each of the perturbation wave vector would then work as eigenfunctions with corresponding eigenvalues Ω, whose imaginary part gives the growth rate. While such a direct approach could be implemented numerically, we here follow a somewhat simpler route where the carrier wave and the Bloch functions are expanded up to the second harmonics, and where the results are more easy to interpret. We mention that in a previous study of the parametric instabilities of electron oscillations due to intense laser light [40], higher order Fourier expansions of the sidebands were employed using Floquet theory (analogous to Bloch theory).

3.1. Stokes waves

Stokes' investigation of water waves (see e.g. [27]) was the starting point of nonlinear theory of dispersive waves, where he among other results found that the dispersion relation involves the wave amplitude. For large amplitude periodic waves, the nonlinearities lead to harmonic generation, where the second harmonics are generated by products of the first harmonics as $\sin^2(\theta_0) = (1 - \cos(2\theta_0))/2$, $\cos^2(\theta_0) = (1 + \cos(2\theta_0))/2$, and $\sin(\theta_0)\cos(\theta_0) = \sin(2\theta_0)/2$, where $\theta_0 = \mathbf{k}_0 \cdot \mathbf{r} - \omega t$ is the phase, $\mathbf{k}_0$ is the wave vector, and ω is the frequency which may depend on the wave amplitude. On the other hand, the beating of the second harmonics by the first harmonics gives $\cos(2\theta_0)\sin(\theta_0) = (-\sin(\theta_0) + \sin(3\theta_0))/2$, $\cos(2\theta_0)\cos(\theta_0) = (\cos(\theta_0) + \cos(3\theta_0))/2$, $\sin(2\theta_0)\sin(\theta_0) = (\cos(\theta_0) - \cos(3\theta_0))/2$, and $\sin(2\theta_0)\cos(\theta_0) = (\sin(\theta_0) + \sin(3\theta_0))/2$. The crucial point is that second harmonic components multiplied by first harmonic components give again components proportional to $\sin(\theta_0)$ and $\cos(\theta_0)$. Such 'secular terms,' which seemed to drive the linear system resonantly, led Stokes to the conclusion that the frequency must change due to nonlinearity. Using a Stokes expansion including first and second harmonics $n_e = n_0 + \hat{n}_{e01}\cos(\theta_0) + \hat{n}_{e02}\cos(2\theta_0)$ and $\psi_e = \hat{\psi}_{e01}\sin(\theta_0) + \hat{\psi}_{e02}\sin(2\theta_0)$ in equations (5) and (6), and separating the equations for the first and second harmonics, gives

$$\text{equation (5)}, \propto \sin(\theta_0): \quad \omega\hat{n}_{e01} - n_0 k_0^2 \hat{\psi}_{e01} - k_0^2 \hat{n}_{e01}\hat{\psi}_{e02} - \frac{1}{2}k_0^2 \hat{n}_{e02}\hat{\psi}_{e01} = 0, \tag{7}$$

$$\text{equation (5)}, \propto \sin(2\theta_0): \quad 2\omega\hat{n}_{e02} - 4n_0 k_0^2 \hat{\psi}_{e02} - k_0^2 \hat{n}_{e01}\hat{\psi}_{e01} = 0, \tag{8}$$

$$\text{equation (6)}, \propto \cos(\theta_0): \quad -\omega\hat{\psi}_{e01} + \frac{g_e \hat{n}_{e01}}{k_0 n_0} + k_0^2 \hat{\psi}_{e01}\hat{\psi}_{e02} = 0, \tag{9}$$

and

$$\text{equation (6)}, \propto \cos(2\theta_0): \quad -2\omega\hat{\psi}_{e02} + \frac{g_e \hat{n}_{e02}}{2k_0 n_0} + \frac{1}{4}k_0^2 \hat{\psi}_{e01}^2 = 0, \tag{10}$$

where we have denoted $g_e = 2D/\epsilon$. Third and higher harmonics were neglected in obtaining equations (7)–(10). Equations (7)–(10) constitute a non-linear eigenvalue problem for $\hat{n}_{e01}$, $\hat{n}_{e02}$, $\hat{\psi}_{e01}$ and $\hat{\psi}_{e02}$, with non-trivial solutions only if the nonlinear dispersion relation

$$\frac{\omega^2}{\omega_0^2} = \frac{(1+Y)^3}{(1-Y)(1-3Y-2Y^2)} \tag{11}$$

is fulfilled, where the nonlinearity is given by

$$Y = \frac{k_0^4 \hat{\psi}_{e01}^2}{2D_2}, \tag{12}$$

and we denoted $D_2 = 4\omega^2 - 2\omega_0^2$, where

$$\omega_0 = \sqrt{g_e k_0}. \tag{13}$$

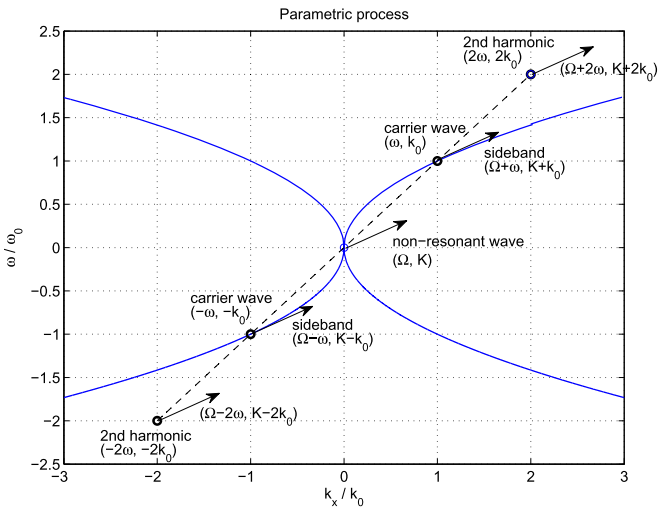

Figure 1. The parametric process, involving the carrier wave at $(\omega,\ \mathbf{k}_0)$ and its second harmonic at $(2\omega,\ 2\mathbf{k}_0)$, the respective sidebands at $(\Omega-\omega,\ \mathbf{K}-\mathbf{k}_0)$, $(\Omega+\omega,\ \mathbf{K}+\mathbf{k}_0)$, $(\Omega-2\omega,\ \mathbf{K}-2\mathbf{k}_0)$, $(\Omega+2\omega,\ \mathbf{K}+2\mathbf{k}_0)$, and a non-resonant driven mode at $(\Omega,\ \mathbf{K})$. Since the dynamic variables are real-valued, the carrier frequency and its second harmonic also occur at $(-\omega,\ -\mathbf{k}_0)$ and $(-2\omega,\ -2\mathbf{k}_0)$, respectively. The solid curve represents the linear dispersion relation $\omega^2=\omega^2(\mathbf{k})\approx g_e k$.

The linear dispersion relation $\omega_0=\sqrt{g_e k_0}$ is of the same form as for deep water gravity waves if g_e is replaced by the gravitational constant g [27–29]. In deriving equation (11), we have used that equations (8)–(10) give the relations

$$\hat{n}_{e02}=2n_0Y\left[1+2\frac{(1-Y)}{(1+Y)}\frac{\omega^2}{\omega_0^2}\right], \tag{14}$$

$$\hat{\psi}_{e02}=\frac{2\omega Y}{k_0^2(1+Y)}, \tag{15}$$

and

$$\hat{n}_{e01}=n_0\frac{(1-Y)}{(1+Y)}\frac{\omega k_0^2\hat{\psi}_{e01}}{\omega_0^2}, \tag{16}$$

which inserted into equation (7) gives equation (11). Equation (11) relates the frequency ω to the wave amplitude $\hat{\psi}_{e01}$. To the lowest order, the frequency depends on the wave amplitude as

$$\omega^2\approx\omega_0^2\left(1+\frac{7}{4}\frac{k_0^4\hat{\psi}_{e01}^2}{\omega_0^2}\right)\approx\omega_0^2\left(1+\frac{7}{4}\frac{\hat{n}_{e01}^2}{n_0^2}\right), \tag{17}$$

which shows a nonlinear upshift of the frequency due to the finite wave amplitude.

3.2. Modulational instability

The stability of the system (5)–(6) is investigated by assuming an expansion of the carrier wave and its sidebands as illustrated in figure 1. The sidebands at $(\Omega\pm\omega,\ \mathbf{K}\pm\mathbf{k}_0)$ are almost resonant, i.e. they are located almost on the dispersion surface of linear waves. The coupling between these almost resonant sidebands by beating of the non-resonant sidebands at $(\Omega,\ \mathbf{K})$ and $(\Omega\pm2\omega,\ \mathbf{K}\pm2\mathbf{k}_0)$ with the large amplitude wave train at $(\omega,\ \mathbf{k}_0)$ and its second harmonic $(2\omega,\ 2\mathbf{k}_0)$ forms a feedback loop which gives rise to a modulational instability for certain values of $\mathbf{K}$. The couplings to second harmonics are crucial to accurately model the modulational instability, and it should be noted that Benjamin and Feir [28] in a similar manner as in figure 1 included the second harmonics in their treatment of the instability of nonlinear water waves. The nonlinear frequency shift is also important, where the carrier frequency ω is given by the nonlinear dispersion relation (11). The dynamical variables in equations (5) and (6) are Fourier expanded including their first and second harmonics, as well as their sidebands, as $n_e=n_0+(1/2)(\hat{n}_{e01}\mathrm{e}^{\mathrm{i}\theta_0}+\hat{n}_{e02}\mathrm{e}^{2\mathrm{i}\theta_0}+\hat{n}_{e+}\mathrm{e}^{\mathrm{i}\theta_+}+\hat{n}_{e-}\mathrm{e}^{\mathrm{i}\theta_-}+\hat{n}_{es}\mathrm{e}^{\mathrm{i}\theta_s}+\hat{n}_{e2+}\mathrm{e}^{\mathrm{i}\theta_{2+}}+\hat{n}_{e2-}\mathrm{e}^{\mathrm{i}\theta_{2-}}+\text{complex conjugate})$ and $\psi_e=(1/2\mathrm{i})(\hat{\psi}_{e01}\mathrm{e}^{\mathrm{i}\theta_0}+\hat{\psi}_{e02}\mathrm{e}^{2\mathrm{i}\theta_0}+\hat{\psi}_{e+}\mathrm{e}^{\mathrm{i}\theta_+}+\hat{\psi}_{e-}\mathrm{e}^{\mathrm{i}\theta_-}+\hat{\psi}_{es}\mathrm{e}^{\mathrm{i}\theta_s}+\hat{\psi}_{e2+}\mathrm{e}^{\mathrm{i}\theta_{2+}}+\hat{\psi}_{e2-}\mathrm{e}^{\mathrm{i}\theta_{2-}})+\text{complex conjugate}$, where $\theta_0=\mathrm{i}\mathbf{k}_0\cdot\mathbf{r}-\mathrm{i}\omega t$, $\theta_s=\mathrm{i}\mathbf{K}\cdot\mathbf{r}-\mathrm{i}\Omega t$, $\theta_\pm=\theta_s\pm\theta_0$, and $\theta_{2\pm}=\theta_s\pm2\theta_0$. The respective Fourier component of the potential is obtained by using equation (2). It is assumed that the sideband components $\hat{n}_{e\pm}$, $\hat{\psi}_{e\pm}$, $\hat{n}_{e2\pm}$, $\hat{\psi}_{e2\pm}$, $\hat{n}_s$, and $\hat{\psi}_s$ have much smaller amplitudes than n_0, $\hat{n}_{e01}$, $\hat{\psi}_{e01}$, $\hat{n}_{e02}$, and $\hat{\psi}_{e02}$, and thus products among sideband components are neglected. The nonlinear wave

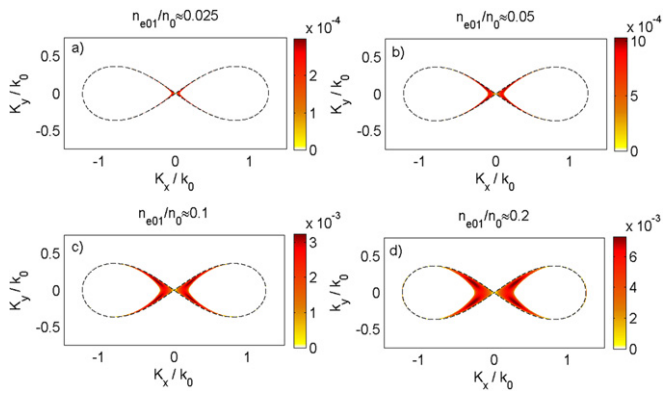

Figure 2. The normalized growth-rate Γ/ω_0 of the modulational instability as a function of the perturbation wave vector (K_x, K_y) for different values of the wave amplitude. The dashed curves indicate the resonance condition (18).

amplitudes $\hat{n}_{e01}$, $\hat{\psi}_{e01}$, $\hat{n}_{e02}$, and $\hat{\psi}_{e02}$ are related to each other through equations (12), (14)–(16). Products between the sidebands and the wavetrain including the carrier wave $\propto e^{\pm i\theta_0}$ and its second harmonic $\propto e^{\pm 2i\theta_0}$ give rise to relations such as $e^{i\theta_-}e^{i\theta_0} = e^{i\theta_s}$, $e^{i\theta_+}e^{-i\theta_0} = e^{i\theta_s}$, $e^{i\theta_-}e^{2i\theta_0} = e^{i\theta_+}$, and $e^{i\theta_+}e^{-2i\theta_0} = e^{i\theta_-}$. Couplings between the second harmonics and the non-resonant sidebands such as $e^{i\theta_{2-}}e^{2i\theta_0} = e^{i\theta_s}$ and $e^{i\theta_{2+}}e^{-2i\theta_0} = e^{i\theta_s}$ are also produced but are numerically found to give only minor contributions to the instability and are therefore neglected here. Separating different Fourier modes gives equations (A1)–(A10) in appendix. The coefficient matrix is on the form of a linear eigenvalue problem for the unknowns $(\hat{n}_{e+}, \hat{\psi}_{e+}, \hat{n}_{e-}, \hat{\psi}_{e-}, \hat{n}_{es}, \hat{\psi}_{es}, \hat{n}_{e2+}, \hat{\psi}_{e2+}, \hat{n}_{e2-}, \hat{\psi}_{e2-})$ where the complex-valued perturbation frequency $\Omega = \Omega_R + i\Gamma$ takes the role of an eigenvalue and where its imaginary part Γ is the growth-rate of the instability.

In the numerical solution of the eigenvalue problem, it is assumed (with no loss of generality) that $\hat{\psi}_{e01}$ is real-valued, which leads to that also $\hat{n}_{e01}$, $\hat{n}_{e02}$ and $\hat{\psi}_{e02}$ are also real-valued and are related to $\hat{\psi}_{e01}$ according to equations (14)–(16); any complex phase factor can be eliminated by a simple change of sideband variables. The wave frequency ω is obtained by solving equation (11) iteratively. A coordinate system is chosen such that the carrier wave propagates in the x-direction, $\mathbf{k}_0 = k_0\hat{\mathbf{x}}$. Amongst the roots given by the system in appendix, we here concentrate on the instability near resonance, where the sidebands $(\omega_\pm, \mathbf{k}_\pm)$ approximately fulfill the linear dispersion relation, so that $\Omega_R \approx (1/2)(\omega_+ - \omega_-) \approx (1/2)(\sqrt{g_e k_+} - \sqrt{g_e k_-})$. The obtained growth-rate for the instability is shown in figure 2 for different wave amplitudes. For small wave amplitudes $\hat{n}_{e01}/n_0 \lesssim 0.1$, the maximum growth-rate depends approximately quadratically on the amplitude, with the maximum growth-rate at an oblique angle to the x-direction. The sidebands have positive growth-rates within a loop-like region in (K_x, K_y)-space obtained from the resonance conditions $\omega_0 = \sqrt{g_e k_0}$, $\omega_+ = \sqrt{g_e k_+}$, and $\omega_- = \sqrt{g_e k_-}$ as

$$\left[\left(\frac{K_x}{k_0} - 1\right)^2 + \left(\frac{K_y}{k_0}\right)^2\right]^{1/4} + \left[\left(\frac{K_x}{k_0} + 1\right)^2 + \left(\frac{K_y}{k_0}\right)^2\right]^{1/4} = 2. \tag{18}$$

The resonance curve is indicated with dashed lines in figure 2. Similar conditions as equation (18) have also been obtained in the theory of nonlinear water waves [41–43]; see for example equation (28) of [43], which in the limit of infinite depth $h \to \infty$ reduces to our equation (18).

4. Nonlinear evolution of the system

The nonlinear evolution of the system is investigated by solving the system (5)–(6) numerically in space and time. The 2D spatial simulation domain $-10\pi \leqslant k_0 x \leqslant 10\pi$ and $-10\pi \leqslant k_0 y \leqslant 10\pi$ is resolved on a numerical grid with 250 intervals in each direction, and with periodic boundary conditions. A pseudospectral method is employed to accurately calculate spatial derivatives, and to obtain the potential by using the formula (2) in Fourier space. The standard 4th-order Runge–Kutta method is used to advance the solution in time with the time-step $\Delta t = 0.2\omega_0^{-1}$. Density waves propagating from left to right are excited resonantly to an amplitude about 10% of the background density, seen in figure 3(a). Small amplitude random numbers of the order 10^{-5} of the background density are added to the electron density to seed the instability. After a linear growth-phase, the wavetrain is amplitude modulated and breaks up into a train of obliquely propagating solitary waves, seen in figure 3(b), and later into more chaotic behavior (figure 3(c)), and into wave turbulence on different length-scales (figure 3(d)).

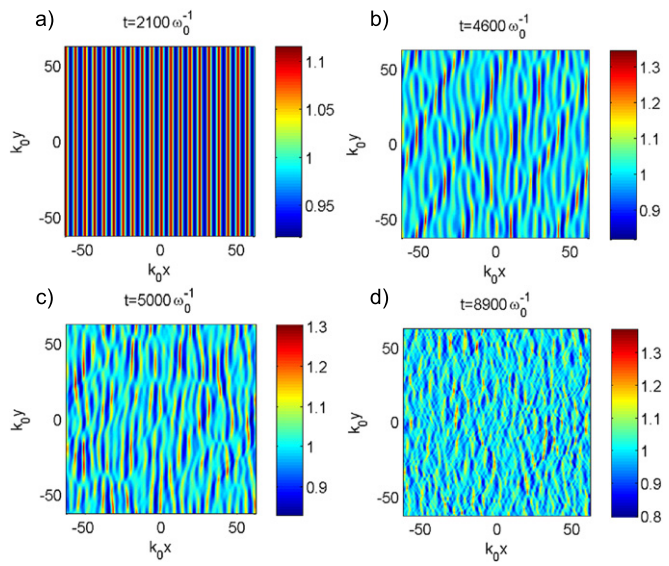

Figure 3. The normalized electron density n_e/n_0 showing (a) a quasi-periodic wavetrain propagating from left to right at time $t = 2100\ \omega_0^{-1}$, (b) modulated obliquely propagating pulses at $t = 4600\ \omega_0^{-1}$, (c) turbulent behavior at $t = 5000\ \omega_0^{-1}$, and (d) a cascade to smaller scales with large amplitude spikes immersed in the turbulence at $t = 8900\ \omega_0^{-1}$.

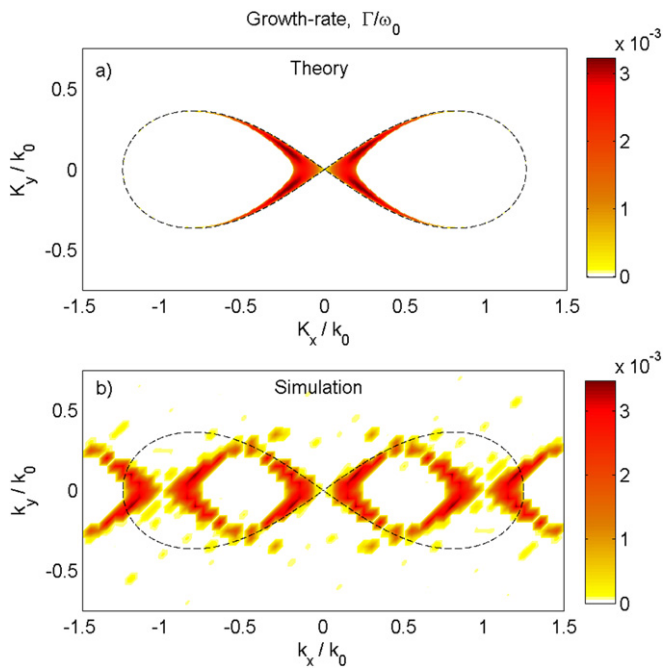

Figure 4. (a) The theoretical growth-rate Γ as a function of (K_x, K_y) for $\hat{n}_{e01}/n_0 \approx 0.1$, and (b) details of the numerically estimated from time-evolution of the wave spectrum of n_e during the linear growth phase of the instability during $t = 1000$–$2000\ \omega_0^{-1}$. Sidebands are formed in a quasi-periodic pattern due to beating with harmonics of the leading wave. The dashed lines are given by the resonance condition (18).

Figure 4 shows a comparison between the theoretical growth-rate (taken from figure 2(c)) with the one estimated from the numerical simulation by doing numerical fits to exponentially growing components of the form $\propto \exp(\Gamma t)$. The theoretical and numeric growth-rates show excellent agreement for small wavenumbers. Due to beating with the harmonics of the carrier wave, ($e^{\pm i\mathbf{k}_0\cdot\mathbf{r}}$, $e^{\pm 2i\mathbf{k}_0\cdot\mathbf{r}}$, etc), the sidebands appear in a quasi-periodic pattern in figure 4(b).

Figure 5 shows a time-series of the electron density n_e at $(x, y) = (0, 0)$. The main features are that the initially periodic wavetrain (see figures 5(a), (b)) becomes unstable and breaks up into a train of localized modulated pulses (figure 5(c)) and density spikes immersed in wave turbulence (figure 5(d)). These spikes have amplitudes several times larger than the mean amplitude of the surrounding waves, which is similar to rogue

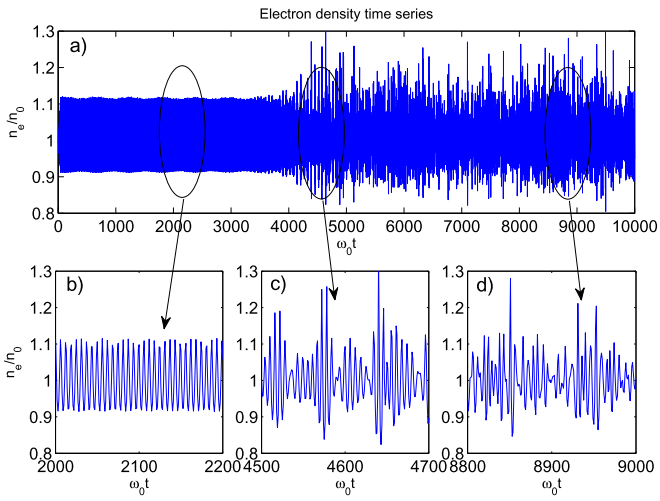

Figure 5. (a) The time-series of the electron density n_e at $(x, y) = (0, 0)$ showing an instability saturating nonlinearly at $t \approx 4500\ \omega_0^{-1}$. Panels (b)—(d) show close-ups at different times. The instability saturates first by the formation of envelope solitary waves (panel (c)) and later isolated, large amplitude pulses (panel (d)).

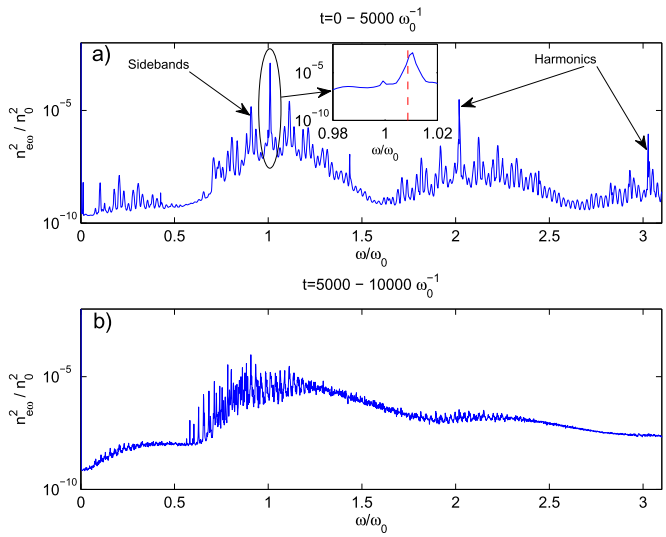

Figure 6. (a) The frequency spectrum $\hat{n}_{e,\omega}$ of the electron density in the time-window $t = 0$–$5000\ \omega_0^{-1}$, showing signatures of harmonic generation and of sidebands to the carrier wave. The inset shows a close-up of frequencies close to the carrier frequency, showing a small frequency upshift of the frequency compared to the linear frequency $\omega = \omega_0$. The vertical dashed line indicates a predicted upshift due to nonlinearity obtained from equation (17). (b) The frequency spectrum has in the time-window $t = 5000$–$10000\ \omega_0^{-1}$ evolved into a broad, continuous spectrum with significant upshifted and downshifted components.

waves on the ocean [29]. Figure 6 shows frequency spectra in time, averaged over all points in the x- and y-directions. The spectrum for earlier times $t = 0$–$5000\ \omega_0^{-1}$ (see figure 6(a)) shows signatures of harmonic generation and smaller amplitude sidebands of the carrier wave. A small upshift of the carrier frequency compared to the linear carrier frequency $\omega = \omega_0$ is also visible in the inset of figure 6(a), which is consistent with the predicted frequency shift due to second harmonic generation given by equation (17) as indicated with a vertical dashed line in the inset. In the fully nonlinear regime shown in figure 6(b) for $t = 5000$–$10000\ \omega_0^{-1}$, the frequency spectrum has evolved into a continuous spectrum with significant components at both higher and lower frequencies compared to $\omega = \omega_0$.

In figure 7, the spatial wave spectrum as a function of (k_x, k_y) is shown at different times. Due to the harmonic generation at multiples of $k_x/k_0 = \pm 1$ and $k_y = 0$, the wave spectrum initially (figure 7(a)) attains a quasi-periodic pattern along the propagation direction. As shown in figures 7(b), (c), the sidebands later grow to large amplitudes and the spectrum widens to both higher and lower wavenumbers. Finally, in figure 7(d), the spectrum is continuous and broad in particular at large wavenumbers.

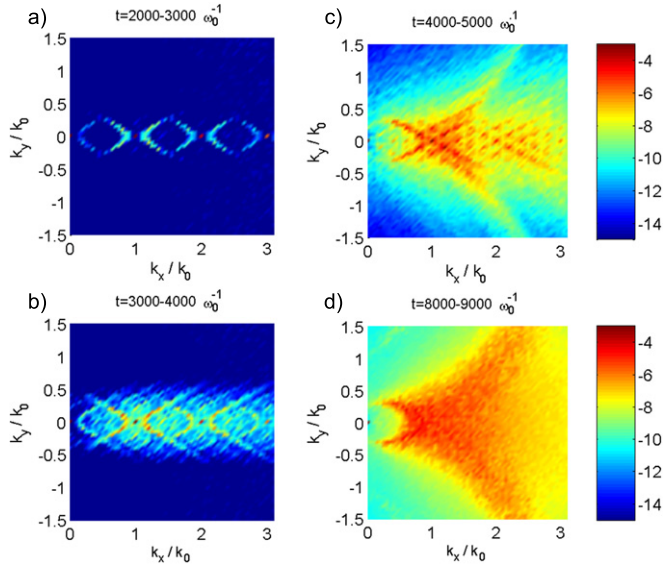

Figure 7. The spatial wave spectrum (10-logarithmic scale) as a function of (k_x, k_y) averaged over different times, showing (a) the linear growth-phase with harmonics and low-amplitude sidebands, (b), (c) sidebands growing to finite amplitudes leading to a broadening of the spectrum, and (d) the fully nonlinear regime with a broad, continuous spectrum.

The regions of instability in figure 2 are to lowest order similar to the ones of the Benjamin–Feir instability of large amplitude water waves modeled by a nonlinear Schrödinger equation; see e.g. figure 12 of [29] and models taking into account higher order nonlinearity and dispersion [43, 44]. Based on the growth-rate of the instability as shown in figure 2, the dynamics may in the limit of long wavelengths/small wavenumbers be phenomenologically modeled by a nonlinear Schrödinger equation of the form

$$\mathrm{i}\left(\frac{\partial A}{\partial t} + c_{gr}\frac{\partial A}{\partial x}\right) + D_x\frac{\partial^2 A}{\partial x^2} + D_y\frac{\partial^2 A}{\partial y^2} - \alpha\omega_0|A|^2 A = 0 \tag{19}$$

where $A = \tilde{n}_e/n_0$ is the normalized complex envelope of the wave, $\tilde{n}_e$ represents the slowly varying envelop of the electron density perturbations, $c_{gr} = \partial\omega/\partial k_x = \omega_0/2k_0$ is the group velocity of the wave train, and the group dispersion coefficients are $D_x = (1/2)\partial^2\omega/\partial k_x^2 = -\omega_0/(8k_0^2)$ and $D_y = (1/2)\partial^2\omega/\partial k_y^2 = \omega_0/(4k_0^2)$ (using $\omega = \sqrt{g_e k}$). The nonlinear Schrödinger equation (19) takes only into account the lowest order dispersive effects, and an assumed cubic nonlinearity amplitude with a coefficient of nonlinearity α. For a monochromatic wave with amplitude $|A| = A_0$, the nonlinear Schrödinger equation (19) supports a modulational instability with the growth-rate $\Gamma = (\omega_0/8k_0^2)\sqrt{16\alpha k_0^2 A_0^2(K_x^2 - 2K_y^2) - (K_x^2 - 2K_y^2)^2}$, which has a maximum of $\Gamma_{\max} = \alpha\omega_0 A_0^2$ for $K_x^2 - 2K_y^2 = 8\alpha k_0^2 A_0^2$. By studying instability diagrams such as figure 2 and recording the maximum growth-rate as a function of amplitude, it is found that the coefficient of nonlinearity α is weakly dependent on nonlinearity and decreases with A_0 as $\alpha \approx 0.53/(1 + 6.5A_0)$ for $A_0 \lesssim 0.1$, giving $\alpha \approx 0.5$ for $A_0 = 0.01$ and $\alpha \approx 0.32$ for $A_0 = 0.1$. It should be mentioned that formal methods of the derivation of the nonlinear Schrödinger equation for general nonlinear systems of equations can be found in [32, 45, 46], for nonlinear water waves in [43, 44], and for plasma waves in [33, 35–39, 47]; we postpone such a formal derivation of the nonlinear Schrödinger equation (19) to a future work.

We next discuss specific examples of experimental parameters in systems of nonlinear 2D plasmons. As a first example, we use parameters for massless Dirac Fermions in graphene [11] with an areal number density of electrons $n_0 = 10^{11}$ cm^{-2} and a wavenumber $k_0 = 0.1k_F$, where the Fermi wavenumber $k_F = \sqrt{\pi n_0} = 5.6 \times 10^5$ cm^{-1}. Using the expressions for the Fermi energy $E_F = \hbar v_F k_F$ (with $v_F = 10^6$ m s^{-1}) and the Drude weight $D = e^2 E_F/(4\pi\epsilon_0\hbar^2)$ then gives the wave frequency $\omega_0 = \sqrt{2Dk_0/\epsilon} = 2.4 \times 10^{13}$ s^{-1} for a graphene layer with one side exposed to air ($\epsilon_1 = 1$) and one side to SiO_2 ($\epsilon_2 = 3.9$) giving $\epsilon = (\epsilon_1 + \epsilon_2)/2 = 2.45$. Using the group speed $c_{gr} = \omega_0/(2k_0) = 2.11 \times 10^8$ cm s^{-1} and the growth-rate for a 10% wave amplitude (see figure 2(c)) $\Gamma = 3 \times 10^{-3}\omega_0 = 7.1 \times 10^{10}$ s^{-1} then gives a gain length of $L_g = c_{gr}/\Gamma \approx 3 \times 10^{-3}$ cm, and the instability would saturate non-linearly within about $10L_g \approx 3 \times 10^{-2}$ cm. The modulational instability typically saturates by initially forming of solitary waves (see figure 2(c)) before breaking up into more complicated structures. As an example, equation (19) supports solitary waves propagating along the x-direction of the form $A = a_0 \mathrm{e}^{\mathrm{i}a_0\alpha t/2}\mathrm{sech}(2a_0\sqrt{\alpha}k_0\xi)$, where $\xi = x - c_{gr}t$. For a 10% nonlinearity ($a_0 = 0.1$) the solitary wave would have an electric field amplitude of (see equation (2))

$|E_x| \sim k_0\phi \sim ea_0 n_0/(2\epsilon_0\epsilon) \sim 4 \times 10^3$ V cm^{-1}, and a pulse width in time of the order $1/(2a_0\sqrt{\alpha}k_0c_{gr}) \sim 10^{-12}$ s. Similar electric field amplitudes ($\sim 10^3$ V cm^{-1}) have been found theoretically for dissipative plasmon solitons in multilayer graphene [25] and graphene nanodisk arrays [26]. As a second example, we consider a plasma layer consisting of an electron sheet on liquid helium [1] with an electron density $n_0 = 10^8$ cm^{-2}. Here the electrons can be treated as Schrödinger electrons which gives the Drude weight $D = e^2n_0/(4\epsilon_0 m_b)$ with the effective mass m_b equal to the free electron mass m_e. A wave frequency $\omega_0 = 2\pi \times 200 \times 10^6$ s^{-1} [1] then gives, using $\omega_0 = \sqrt{2Dk_0/\epsilon}$ with $\epsilon \approx 1$, that $k_0 = 10$ cm^{-1}. Using the growth-rate $\Gamma = 3 \times 10^{-3}\,\omega_0 = 3.8 \times 10^6$ s^{-1} and the group speed $c_{gr} = \omega_0/(2k_0) = 6.3 \times 10^7$ cm s^{-1} gives the gain length $L_g = c_{gr}/\Gamma = 17$ cm. Typical experimental plasmas involving sheets of electrons on liquid helium have sizes of a few centimeters, which is probably too small to observe the modulational instability in a single pass. However, the modulational instability could potentially develop in the standing wave generated by repeated reflections of the wave against the edges of the plasma.

5. Conclusions and discussion

In conclusion, we have investigated the nonlinear behavior of plasmons in a 2D plasma layer. For a periodic large-amplitude wave, the harmonic generation leads to a nonlinear upshift of the frequency. The large amplitude wave-train is subject to a modulational instability that leads to the growth of sidebands and modulation of the periodic wavetrain. The linear dispersion of the 2D plasmons, as well as their nonlinear frequency upshift and modulational instability, have an interesting analogy in gravity waves such as ocean waves. Direct numerical simulations of the dynamical system confirm both the predicted nonlinear upshift of the frequency and the growth-rate of the modulational instability. The wavetrain eventually breaks up into a series of modulated pulses and more complicated wave turbulence. The spatial and temporal wave spectra show a dual cascade of wave energy to both higher and lower frequencies associated with components at both smaller and larger length-scales.

It has been suggested in the past [34] that large amplitude electron plasma waves in 3D cold electron gaseous plasmas with fixed ions also can undergo a parametric instability with a redistribution of energy from large scales to small-scale sidebands. We carried out a simulation (not shown) similar to that in figure 3 for this case but could not see any sign of instability. Hence, it seems that the 2D geometry is crucial for the modulational instability of plasmons involving only electrons. In a 3D electron-ion plasma, due to the very low group velocity of the electron oscillations, the coupling to the ion dynamics instead leads to Langmuir wave collapse and strong turbulence [48, 49] via the ponderomotive pressure acting on the electrons on a slow time-scale.

Our results show that a modulational instability for plasmons involving massless Dirac fermions in graphene with 10% density variations compared to the background density could give rise to a modulational instability on a typical typical time-scale of the order of a nanosecond and a length-scale of the order 10^{-3} cm. The instability would give rise to large amplitude spikes emersed in wave turbulence, similar as has been observed in optical systems [22, 23]. With the advances in graphene fabrication [50], such experiments could potentially be realized in near future.

Acknowledgments

BE acknowledges the hospitality of University of Macau, Macau, PR China, where this work was carried out. This work was partially supported by the EPSRC (UK), grant EP/M009386/1. Discussions with V K Tripathi are gratefully appreciated. The simulation data associated with this paper are available at: http://dx.doi.org/10.15129/fb2ab071-2ed2-4718-aafd-c56315764b97.

Appendix. Coupling equations for the sidebands

Separating different Fourier modes in equations (5) and (6) gives the equations for the coefficients of the sidebands as

equation (5), $\propto e^{i\theta_+}$:

$$-\omega_+\hat{n}_{e+} + n_0k_+^2\hat{\psi}_{e+} + \frac{1}{2}\mathbf{k}_+\cdot\mathbf{K}\hat{n}_{e01}\hat{\psi}_{es} + \frac{1}{2}\mathbf{k}_+\cdot\mathbf{k}_0\hat{\psi}_{e01}\hat{n}_{es}$$
$$+\frac{1}{2}\mathbf{k}_+\cdot\mathbf{k}_-\hat{n}_{e02}\hat{\psi}_{e-} + \mathbf{k}_+\cdot\mathbf{k}_0\hat{\psi}_{e02}\hat{n}_{e-} + \frac{1}{2}\mathbf{k}_+\cdot\mathbf{k}_{2+}\hat{n}_{e01}^*\hat{\psi}_{e2+} + \frac{1}{2}\mathbf{k}_+\cdot\mathbf{k}_0\hat{\psi}_{e01}^*\hat{n}_{e2+} = 0 \quad \text{(A1)}$$

equation (6), $\propto e^{i\theta_+}$:

$$-\omega_+\hat{\psi}_{e+} + \frac{g_e\hat{n}_{e+}}{k_+n_0} + \frac{1}{2}\mathbf{k}_0\cdot\mathbf{K}\hat{\psi}_{e01}\hat{\psi}_{es} + \mathbf{k}_-\cdot\mathbf{k}_0\hat{\psi}_{e02}\hat{\psi}_{e-} + \frac{1}{2}\mathbf{k}_0\cdot\mathbf{k}_{2+}\hat{\psi}^*_{e01}\hat{\psi}_{e2+} = 0 \tag{A2}$$

equation (5), $\propto e^{i\theta_-}$:

$$\begin{aligned}&-\omega_-\hat{n}_{e-} + n_0k_-^2\hat{\psi}_{e-} + \frac{1}{2}\mathbf{k}_-\cdot\mathbf{K}\hat{n}^*_{e01}\hat{\psi}_{es} + \frac{1}{2}\mathbf{k}_-\cdot\mathbf{k}_0\hat{\psi}^*_{e01}\hat{n}_{es}\\&+\frac{1}{2}\mathbf{k}_+\cdot\mathbf{k}_-\hat{n}^*_{e02}\hat{\psi}_{e+} + \mathbf{k}_-\cdot\mathbf{k}_0\hat{\psi}^*_{e02}\hat{n}_{e+} + \frac{1}{2}\mathbf{k}_-\cdot\mathbf{k}_{2-}\hat{n}_{e01}\hat{\psi}_{e2-} + \frac{1}{2}\mathbf{k}_-\cdot\mathbf{k}_0\hat{\psi}_{e01}\hat{n}_{e2-} = 0\end{aligned} \tag{A3}$$

equation (6), $\propto e^{i\theta_-}$:

$$-\omega_-\hat{\psi}_{e-} + \frac{g_e\hat{n}_{e-}}{k_-n_0} + \frac{1}{2}\mathbf{k}_0\cdot\mathbf{K}\hat{\psi}^*_{e01}\hat{\psi}_{es} + \mathbf{k}_+\cdot\mathbf{k}_0\hat{\psi}^*_{e02}\hat{\psi}_{e+} + \frac{1}{2}\mathbf{k}_0\cdot\mathbf{k}_{2-}\hat{\psi}_{e01}\hat{\psi}_{e2-} = 0 \tag{A4}$$

equation (5), $\propto e^{i\theta_s}$:

$$-\Omega\hat{n}_{es} + n_0K^2\hat{\psi}_{es} + \frac{1}{2}\mathbf{k}_-\cdot\mathbf{K}\hat{n}_{e01}\hat{\psi}_{e-} + \frac{1}{2}\mathbf{k}_+\cdot\mathbf{K}\hat{n}^*_{e01}\hat{\psi}_{e+} + \frac{1}{2}\mathbf{k}_0\cdot\mathbf{K}\hat{\psi}_{e01}\hat{n}_{e-} + \frac{1}{2}\mathbf{k}_0\cdot\mathbf{K}\hat{\psi}^*_{e01}\hat{n}_{e+} = 0 \tag{A5}$$

equation (6), $\propto e^{i\theta_s}$:

$$-\Omega\hat{\psi}_{es} + \frac{g_e\hat{n}_{es}}{Kn_0} + \frac{1}{2}\mathbf{k}_-\cdot\mathbf{k}_0\hat{\psi}_{e01}\hat{\psi}_{e-} + \frac{1}{2}\mathbf{k}_+\cdot\mathbf{k}_0\hat{\psi}^*_{e01}\hat{\psi}_{e+} = 0 \tag{A6}$$

equation (5), $\propto e^{i\theta_{2+}}$:

$$-\omega_{2+}\hat{n}_{e2+} + n_0k_{2+}^2\hat{\psi}_{e2+} + \frac{1}{2}\mathbf{k}_{2+}\cdot\mathbf{k}_+\hat{n}_{e01}\hat{\psi}_{e+} + \frac{1}{2}\mathbf{k}_{2+}\cdot\mathbf{k}_0\hat{\psi}_{e01}\hat{n}_{e+} = 0 \tag{A7}$$

equation (6), $\propto e^{i\theta_{2+}}$:

$$-\omega_{2+}\hat{\psi}_{e2+} + \frac{g_e\hat{n}_{e2+}}{k_{2+}n_0} + \frac{1}{2}\mathbf{k}_0\cdot\mathbf{k}_+\hat{\psi}_{e01}\hat{\psi}_{e+} = 0 \tag{A8}$$

equation (5), $\propto e^{i\theta_{2-}}$:

$$-\omega_{2-}\hat{n}_{e2-} + n_0k_{2-}^2\hat{\psi}_{e2-} + \frac{1}{2}\mathbf{k}_{2-}\cdot\mathbf{k}_-\hat{n}^*_{e01}\hat{\psi}_{e-} + \frac{1}{2}\mathbf{k}_{2-}\cdot\mathbf{k}_0\hat{\psi}^*_{e01}\hat{n}_{e-} = 0 \tag{A9}$$

equation (6), $\propto e^{i\theta_{2-}}$:

$$-\omega_{2-}\hat{\psi}_{e2-} + \frac{g_e\hat{n}_{e2-}}{k_{2-}n_0} + \frac{1}{2}\mathbf{k}_0\cdot\mathbf{k}_-\hat{\psi}^*_{e01}\hat{\psi}_{e-} = 0 \tag{A10}$$

where $\mathbf{k}_\pm = \mathbf{K} \pm \mathbf{k}_0$, $\omega_\pm = \Omega \pm \omega$, $\mathbf{k}_{2\pm} = \mathbf{K} \pm 2\mathbf{k}_0$, and $\omega_{2\pm} = \Omega \pm 2\omega$.

References

[1] Grimes C C and Adams G 1976 Observation of two-dimensional plasmons and electron-ripplon scattering in a sheet of electrons on liquid helium *Phys. Rev. Lett.* **36** 145–8

[2] Allen S J Jr, Tsui D C and Logan A R 1977 Observation of the two-dimensional plasmon in silicon inversion layers *Phys. Rev. Lett.* **38** 980–3

[3] Nagashima A, Nuka K, Itoh H, Ichinokawa T, Oshima C, Otani S and Ishizawa Y 1992 Two-dimensional plasmons in monolayer graphite *Solid State Commun.* **83** 581–5

[4] Liu Y, Willis R F, Emtsev K V and Seyller T 2008 Plasmon dispersion and damping in electrically isolated two-dimensional charge sheets *Phys. Rev.* B **78** 201403(R)

[5] Shin S Y, Kim N D, Kim J G, Kim K S, Noh D Y, Kim Kwang S and Chung J W 2011 Control of the π plasmon in a single layer graphene by charge doping *Appl. Phys. Lett.* **99** 082110

[6] Lu J, Loh K P, Huang H, Chen W and Wee A T S 2009 Plasmon dispersion on epitaxial graphene studied using high-resolution electron energy-loss spectroscopy *Phys. Rev.* B **80** 113410

[7] Novoselov K S, Geim A K, Morozov S V, Jiang D, Zhang Y, Dubonos S V, Grigorieva I V and Firsov A A 2004 Electric field effect in atomically thin carbon films *Science* **306** 666–9

[8] Novoselov K S, Jiang D, Schedin F, Booth T J, Khotkevich V V, Morozov S V and Geim A K 2005 Two-dimensional atomic crystals *Proc. Natl Acad. Sci. USA* **102** 10451–3

[9] Novoselov K S, Geim A K, Morozov S V, Jiang D, Katsnelson M I, Grigorieva I V, Dubonos S V and Firsov A A 2005 Two-dimensional gas of massless Dirac fermions in graphene *Nature* **438** 197–200

[10] Ulstrup S *et al* 2014 Ultrafast dynamics of massive Dirac fermions in bilayer graphene *Phys. Rev. Lett.* **112** 257401

[11] Grigorenko A N, Polini M and Novoselov K S 2012 Graphene plasmonics *Nat. Photon.* **6** 749–58

[12] Luo X, Qiu T, Lu W and Ni Z 2013 Plasmons in graphene: recent progress and applications *Mater. Sci. Eng.* R **74** 351–76

[13] Koch R J, Seyller T and Schaefer J A 2010 Strong phonon-plasmon coupled modes in the graphene/silicon carbide heterosystem *Phys. Rev.* B **82** 201413

[14] Mikhailov S A 2007 Non-linear electromagnetic response of graphene *Europhys. Lett.* **79** 27002

[15] Peres N M R, Bludov Yu V, Santos J E, Jauho A-P and Vasilevskiy M I 2014 Optical bistability of graphene in the terahertz range *Phys. Rev.* B **90** 125425
[16] Christensen T, Yan W, Jauho A-P, Wubs M and Mortensen N A 2015 Kerr nonlinearity and plasmonic bistability in graphene nanoribbons *Phys. Rev.* B **92** 121407(R)
[17] Wang J, Hernandez Y, Lotya M, Coleman J N and Blau Werner J 2009 Broadband nonlinear optical response of graphene dispersions *Adv. Mater.* **21** 2430–5
[18] Wu Y *et al* 2015 Generation of cascaded four-wave-mixing with graphene-coated microfiber *Photon. Res.* **3** A64–8
[19] Yamashita S 2012 A tutorial on nonlinear photonic applications of carbon nanotube and graphene *J. Lightwave Technol.* **30** 427–47
[20] Yahia M E, Tolba R E, El-Bedwehy N A, El-Labany S K and Moslem W M 2015 Rogue waves lead to the instability in GaN semiconductors *Sci. Rep.* **5** 12245
[21] Zamora-Munt J, Garbin B, Barland S, Giudici M, Leite J R R, Masoller C and Tredicce J R 2013 Rogue waves in optically injected lasers: Origin, predictability, and suppression *Phys. Rev.* A **87** 035802
[22] Solli D R, Ropers C, Koonath P and Jalali B 2007 Optical rogue waves *Nature* **450** 1054–7
[23] Montina A, Bortolozzo U, Residori S and Arecchi F T 2009 Non-Gaussian statistics and extreme waves in a nonlinear optical cavity *Phys. Rev. Lett.* **103** 173901
[24] Nesterov M L, Bravo-Abad J, Yu A, Nikitin F J, García-Vidal and Martin-Moreno L 2013 Graphene supports the propagation of subwavelength optical solitons *Laser Photon. Rev.* **7** L7–11
[25] Smirnova D A, Shadrivov I V, Smirnov A I and Kivshar Y S 2014 Dissipative plasmon-solitons in multilayer graphene *Laser Photon. Rev.* **8** 291–6
[26] Smirnova D A, Noskov R E, Smirnov L A and Kivshar Y S 2015 Dissipative plasmon solitons in graphene nanodisk arrays *Phys. Rev.* B **91** 075409
[27] Whitham G B 1974 *Linear and Nonlinear Waves* (New York: Wiley)
[28] Benjamin T B and Feir J E 1967 The disintegration of wave trains on deep water: 1. Theory *J. Fluid Mech.* **27** 417–30
[29] Kharif C and Pelinovsky E 2003 Physical mechanisms of the rogue wave phenomenon *Eur. J. Mech. B Fluids* **22** 603–34
[30] Giuliani G F and Vignale G 2005 *Quantum Theory of the Electron Liquid* (Cambridge: Cambridge University Press)
[31] Abedinpour S H, Vignale G, Principi A, Polini M, Tse W-K and MacDonald A H 2011 Drude weight, plasmon dispersion, and ac conductivity in doped graphene sheets *Phys. Rev.* B **84** 045429
[32] Karpman V I and Krushkal E M 1969 Modulated waves in nonlinear dispersive media *Soviet Phys. J. High Energy Phys.* **28** 277–81
[33] Kakutani T and Sugimoto N 1974 Krylov-Bogoliubov-Mitropolsky method for nonlinear wave modulation *Phys. Fluids* **17** 1617–25
[34] Sturrock P A 1957 Non-linear effects in electron plasmas *Proc. R. Soc. Lond.* A **242** 277–99
Sturrock P A 1961 *Nucl. Energy Part C: Plasma Phys.* **2** 158–63
[35] Hasegawa A 1970 Stimulated modulational instabilities of plasma waves *Phys. Rev.* A **1** 1746–50
[36] Kourakis I and Shukla P K 2005 Exact theory for localized envelope modulated electrostatic wavepackets in space and dusty plasmas *Nonlin. Proc. Geophys* **12** 407–23
[37] Kourakis I and Shukla P K 2005 Nonlinear propagation of electromagnetic waves in negative-refraction-index composite materials *Phys. Rev.* E **72** 016626
[38] Sultana S and Kourakis I 2011 Electrostatic solitary waves in the presence of excess superthermal electrons: modulational instability and enveloüe soliton modes *Plasma Phys. Control. Fusion* **53** 045003
[39] McKerr M, Kourakis I and Haas F 2014 Freak waves and electrostatic wavepacket modulation in a quantum elecron-positron-ion plasma *Plasma Phys. Control. Fusion* **56** 035007
[40] Quesnel B, Mora P, Adam J C, Héron A and Laval G 1997 Electron parametric instabilities of ultraintense laser pulses propagating in plasmas of arbitrary density *Phys. Plasmas* **4** 3358–68
[41] Phillips O M 1960 On the dynamics of unsteady gravity waves of finite amplitude: 1. The elementary interactions *J. Fluid Mech.* **9** 193–217
[42] McLean J W 1982 Instabilities of finite-amplitude gravity waves on water of finite depth *J. Fluid Mech.* **114** 331–41
[43] Trulsen K and Dysthe K B 1996 A modified nonlinear Schrödinger equation for broader bandwidth gravity waves on deep water *Wave Motion* **24** 281–9
[44] Dysthe K B 1979 Note on a modification to the nonlinear Schrödinger equation for application to deep water waves *Proc. R. Soc. Lond.* A **369** 105–14
[45] Taniuti T and Yajima N 1969 Perturbation method for a nonlinear wave modulation *I, J. Math. Phys.* **10** 1369–72
[46] Asano N, Taniuti T and Yajima N 1969 Perturbation method for a nonlinear wave modulation *II, J. Math. Phys.* **10** 2020–4
[47] Sen A, Karney C F F, Johnston G L and Bers A 1978 Three-dimensional effects in the non-linear propagation of lower-hybrid waves *Nucl. Fusion* **18** 171–9
[48] Zakharov V E 1972 Collapse of Langmuir waves *Soviet Phys. J. High Energy Phys.* **35** 908–14
[49] Thornhill S G and ter Haar D 1978 Langmuir turbulence and modulational instability *Phys. Rep.* **43** 43–99
[50] McNerny D Q, Viswanath B, Copic D, Laye F R, Prohoda C, Brieland-Shoultz A C, Polsen E S, Dee N T, Veerasamy V S and Hart J 2014 Direct fabrication of graphene on SiO_2 enabled by thin film stress engineering *Sci. Rep.* **4** 5049